Electronic Supplementary Material (ESI) for ChemComm.

Electronic Supporting Information

Asymmetric coupling of Au nanospheres on TiO_2 nanochannels membrane for NIR-gated artificial ionic nanochannels

Lingling Yang,[a] Kuanzhi Qu,[a] Junli Guo,[a] Huijie Xu,[a] Zhenqing Dai,[a] Zhi-Da Gao,*[a] Yan-Yan Song*[a]

College of Sciences, Northeastern University, Shenyang 110004, China
E-mail addresses: gaozd@mail.neu.edu.cn; yysong@mail.neu.edu.cn

Table of contents

1. Experimental

1.1 Materials.

Ti sheets (0.1 mm thickness, 99.6 % purity) were purchased from Baosheng Hardware Co. Ltd (Bao ji, China). Ammonium fluoride (NH_4F), ethylene glycol, and other chemicals were purchased from Sinopharm Chemical Reagent Co. Ltd. 3-Aminopropyltriethoxysilane (APTES), 2-bromoisobutyryl bromide (BIBB), *N*-isopropylacrylamide (NIPAAm), 1,1,4,7,7-pentamethyldiethylenetriamine (PMDETA), and Cu(I) chloride were obtained from Aladdin. The chemical reagents were used as received without further purification. The NIPAAm was recrystallized from a mixture of toluene and *n*-hexane (1:3, v/v) before use. All other chemicals used in this study were of analytical grade and used as received without further purification. All the solutions were prepared in deionized (DI) water (18.2 MΩ).

1.2 Characterization

The morphological characterization was carried out using a field-emission scanning electron microscope (FESEM SU 8000, Japan). The XRD patterns were acquired on an X'Pert X-ray diffraction spectrometer (Philips, USA) using a CuKα X-ray source. Ion current was measured using a Keithley 6487 picoammeter (Keithley Instruments, Cleveland, OH). Ag/AgCl electrodes were used to apply a transmembrane voltage across the nanochannels because of their high sensitivity and good stability. UV/visible diffuse reflectance spectra were obtained using a Perkin-Elmer spectrometer (Lambda 750S, USA). Zeta potentials of NPs were measured using a nano zetasizer (Nano zs90 Malvin Instruments). X-ray photoelectron spectra (XPS) was recorded on a Perkin–Elmer Physical Electronics 5600 spectrometer using Al Ka radiation at 13 kV as excitation source. The takeoff angle of the emitted photoelectrons was 45°, and the binding energy of the target elements was determined at a pass energy of 23.5 eV with a resolution of 0.1 eV. The binding energy of Ti 2p signal (458.0 eV)[1] of bulk TiO_2 was used as the reference.

1.3 Preparation of Au/TiNM

The Ti foils (15 mm × 15 mm × 0.1 mm) were first sonicated in isopropanol, ethanol, and DI water and then dried under a stream of N_2 gas. The open-ended TiNM were prepared using electrochemical anodizing method in an electrolyte of ethylene glycol/lactic acid/water /NH_4F at 120 V for 20 min, and then the TiO_2 nanotubes were detached from the Ti substrate in H_2O_2 (30%).[2] The resulting TiNM was annealed at 450 °C in air. To modify AuNPs on TiNM, the TiNM was immersed in an alkaline $HAuCl_4$ solution[3] for 12 h and then cleaned with DI water. Then, the TiNM was exposed under a mercury lamp (500 W)[4] for 3 min to decorate AuNPs on TiNM (Au/TiNM).

1.4 Grafted PNIPAAm on TiNM and Au/TiNM

To grafted PNIPAAm, the TiNM or Au/TiNM was first immersed in a 10 mM APTES toluene solution. The reaction was carried out for 12 h at 70 °C to obtain many NH_2 groups on TiNM; the TiNM or Au/TiNM was thoroughly washed with acetone and dried under RT to remove the physically absorbed APTES.[1] Next, the resulting APTES-decorated TiNM or Au/TiNM was illuminated under a mercury lamp (500 W) for 30 min to remove the NH_2 groups at the large-base side of TiNM or Au/TiNM, thoroughly washed with ethanol and water, and dried. Next, the asymmetrically decorated TiNM or Au/TiNM with NH_2 groups was transferred into 792 µl of anhydrous DCM and 8 µl anhydrous Et_3N. Next, 8 µl BIBB was added into the above mixture on an ice bath and ultrasonicated for 5 min. The reaction was left overnight at RT. The resulting membrane with Br groups was then cleaned with acetone and ethanol, followed by drying under a stream of N_2 gas. Polymerization of NIPAAm was achieved by immersing the TiNM or Au/TiNM in a degassed solution in 1:1 (v/v) mixture of H_2O and CH_3OH (800 µl) containing NIPAAm (80 mg), CuCl (2.6 mg), and PMDETA (11.2 µl) for 30 min at 60 °C.[5] Then, the TiNM was washed thoroughly with pure H_2O and stored in H_2O at RT.

1.5 Photothermal conversion tests

The TiNM and Au/TiNM are circular membranes with a diameter of 8 mm. The samples were irradiated with an 808-nm laser at a power density of 1 W cm^{-2} at RT. To evaluate the temperature rise on the surface of Au/TiNM and TiNM, only 100 µl water was added to achieve a situation as close as possible to the real situation. The temperature data were recorded using an FILR E40 instrument.

1.6 Numerical simulation.

Numerical simulation was performed using commercial software Lumerical FDTD Solutions. For studying the TiO_2 and AuNPs, a perfectly matched layer was used as the boundary condition for the simulation studies. The permittivity of Au in the NIR regime can be described by the Lorentz−Drude model. The radius of Au nanoparticle is 20 nm and 100 nm.

1.7 Electrochemical measurements.

The nanochannel membrane was mounted between two halves of a conductivity cell, and each half-cell was filled with 1 mM KCl solution. The current was measured using a Keithley 6487 picoammeter voltage source (Keithley Instruments). A pair of homemade Ag/AgCl electrodes was settled in each half-cell to apply the desired transmembrane potential and to measure the resulting ionic current. The main transmembrane potential used in this study was a scanning voltage varying from –1 V to +1 V with a 5 s period. The membrane was mounted between two halves of the conductance cell. The effective membrane area for current recording is about 3.14 mm^2.

2. Supplementary Figures

SEM images and EDS results

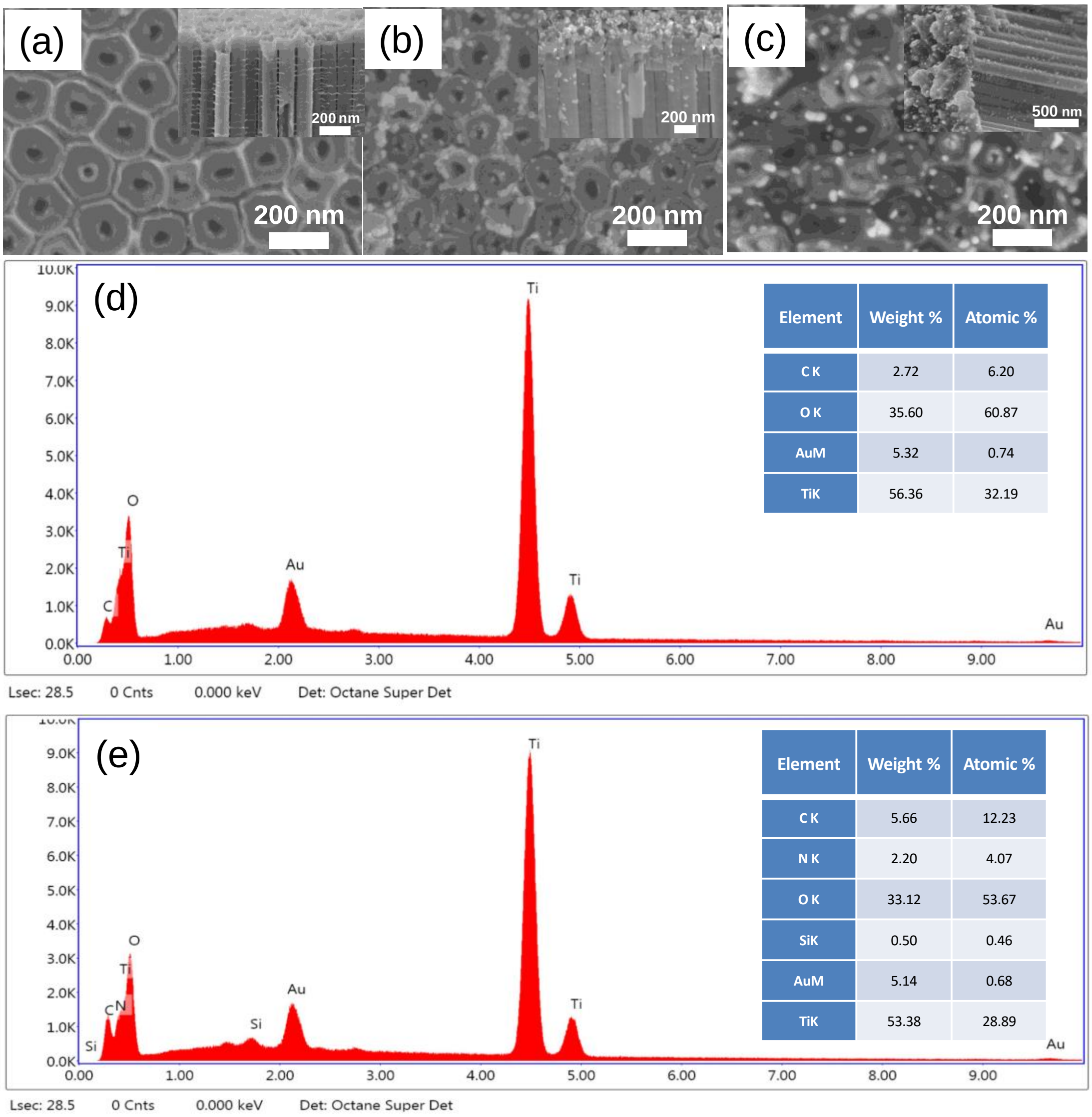

(d)

Element	Weight %	Atomic %
C K	2.72	6.20
O K	35.60	60.87
AuM	5.32	0.74
TiK	56.36	32.19

(e)

Element	Weight %	Atomic %
C K	5.66	12.23
N K	2.20	4.07
O K	33.12	53.67
SiK	0.50	0.46
AuM	5.14	0.68
TiK	53.38	28.89

Fig. S1. SEM images of top-view and cross-sectional view for the tip-side of (a) TiNM, (b) Au/TiNM, and (c) PNIPAAm grafted Au/TiNM. The EDS results of Au/TiNM (d) without and (e) with PNIPAAm modification.

XPS patterns of Au/TiNM

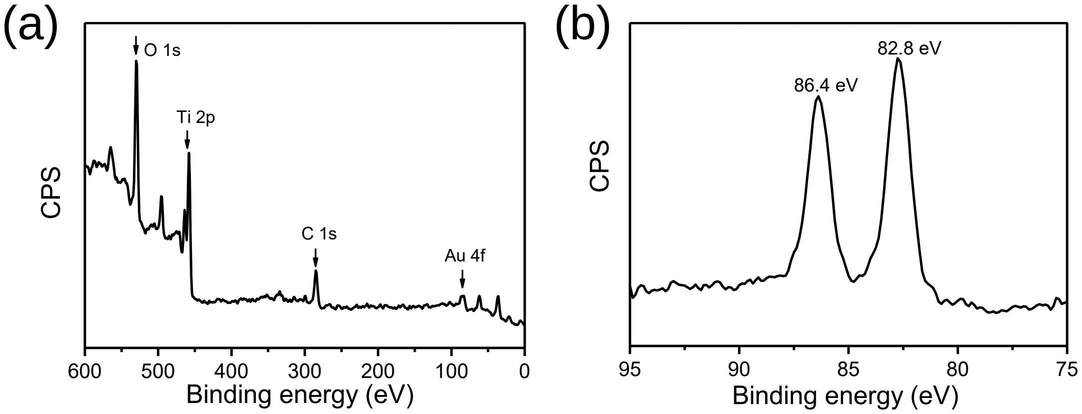

Fig. S2 XPS analysis of Au/TiNM (a) survey spectra, and (b) high resolution Au 4f signal. CPS = counts per second.

XRD patterns

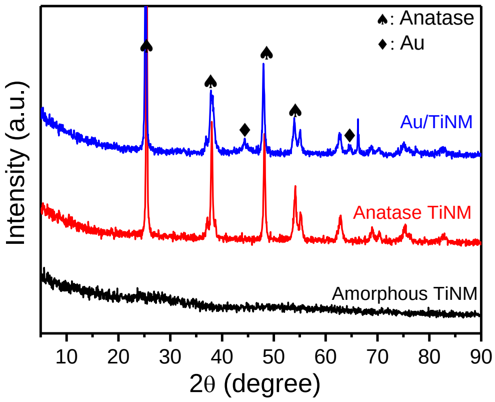

Fig. S3. XRD patterns of amorphous TiNM, anatase TiNM, and Au/TiNM.

XPS patterns of Au/TiNM/APTES and Au/TiNM/APTES/PNIPAAm

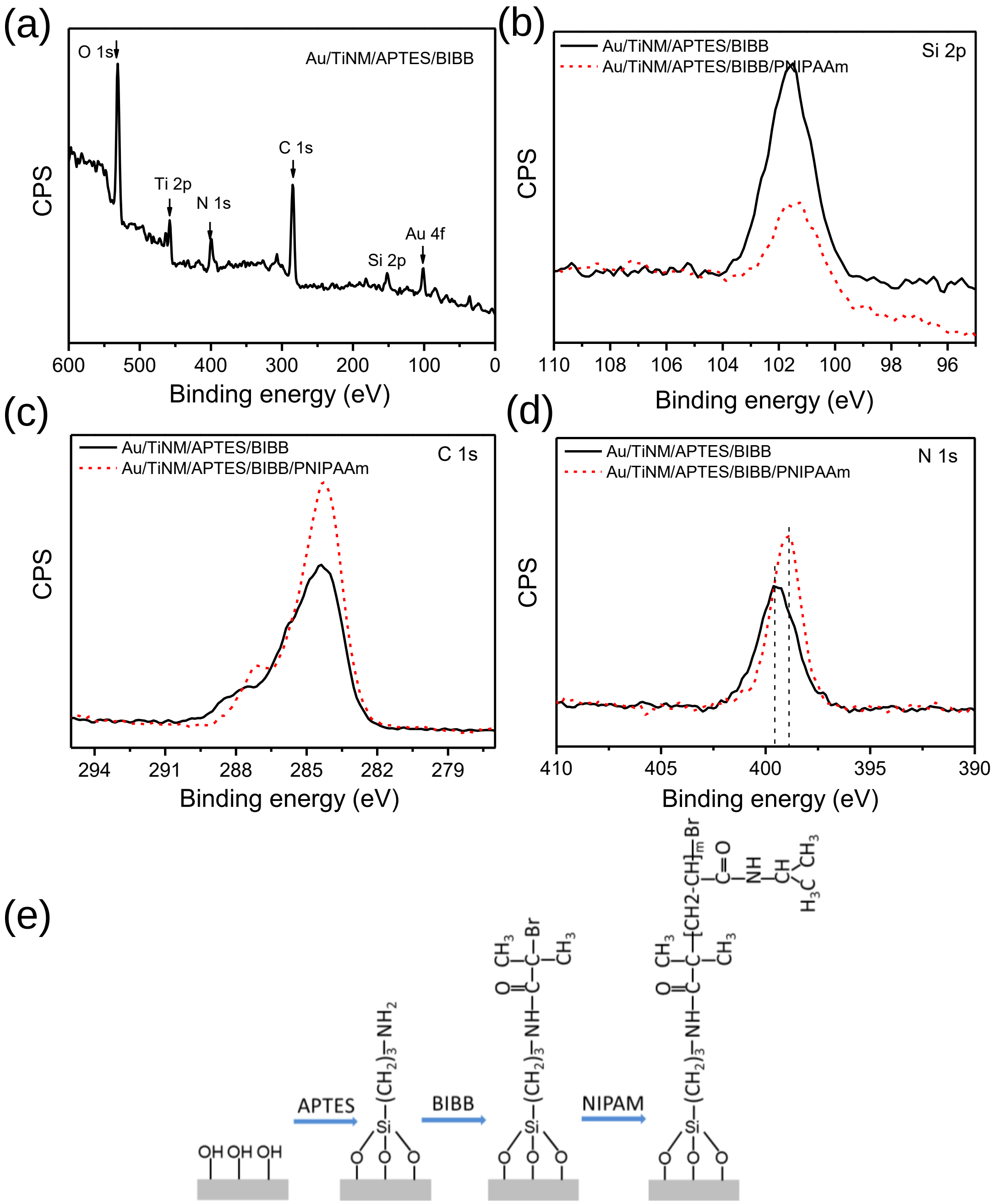

Fig. S4 (a) XPS survey spectra of Au/TiNM/APTES/BIBB, and high resolution XPS spectra of (b) Si 2p, (c) C 1s, and (d) N 1s before (black curve) and after (red curve) PNIPAAm modification. CPS = counts per second. (e) Schematic illustration of grafted PNIPAAm chains.

To further investigate the successful attachment of PNIPAAm, XPS was employed to characterize the change of surface composition before and after PNIPAAm modification. As APTES contains C and N elements (Fig. S4e), we compared the element changes in Si 2p, C 1s and N 1s signals of Au/TiNM/APTES/BIBB before and after PNIPAAm modification. Fig. S4a shows that a monolayer of APTES successfully attached to the Au/TiNM–this by the apparently increased signals of Si 2p and N 1s.[6] After modifying PNIPAAm, an obvious decrease of the Si 2p peak is observed (Fig. S4b) due to the coverage of PNIPAAm. Meanwhile, the enhancement of C 1s (Fig. S4c) and

N 1s (Fig. S4d) signals can be seen by PNIPAAm coating. Furthermore, in Fig. S4d, an obvious enhancement of signal intensity and slight shift the peak can be noticed for N 1s, which can be ascribed to the N content in PNIPAAm. These XPS results demonstrate the successful attachment of PNIPAAm layer on the membrane.

Photographs of water droplet

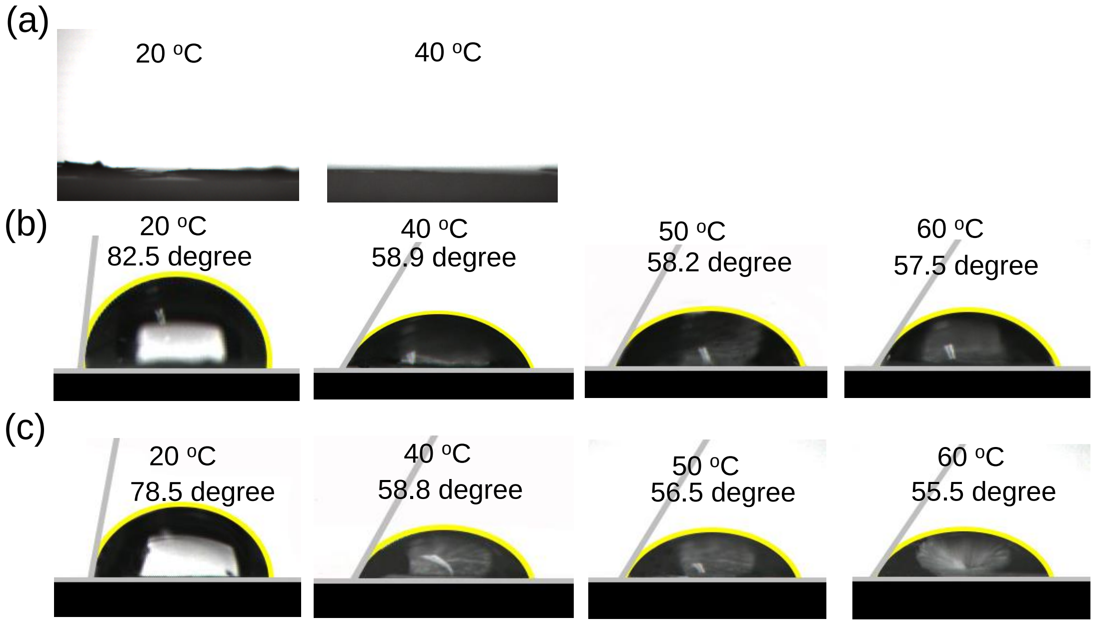

Fig. S5 **Influence of temperature on the wettability.** Photographs of water droplet on (a) unmodified Au/TiNM, (b) PNIPAAm-modified Au/TiNM, and (c) PNIPAAm-modifed TiNM at different temperatures. (These experiment are carried out by controlling the surrounding environment and substrate temperature)

As shown in Fig. S5, the bare Au/TiNM is hydrophilic; the contact angle almost does not change with the temperature increase from 20 °C to 40 °C.

For PNIPAAm-modified Au/TiNM (Fig. S5b), the contact angle is ~82.5° at 20 °C (Fig. S5b). The contact angle decreases to ~58.9° when the substrate temperature increases to 40 °C. And the contact angle dosen't exhibit significant change after the temperature elevate to 50 °C and 60 °C. These results clearly indicate that the PNIPAAm exhibit a good temperature response.

For PNIPPAm modified TiNM (Fig. 5c), the contact angles show the similar tendency as PNIPAAm-modified Au/TiNM in Fig. S5b.

UV/visible diffuse reflectance spectra

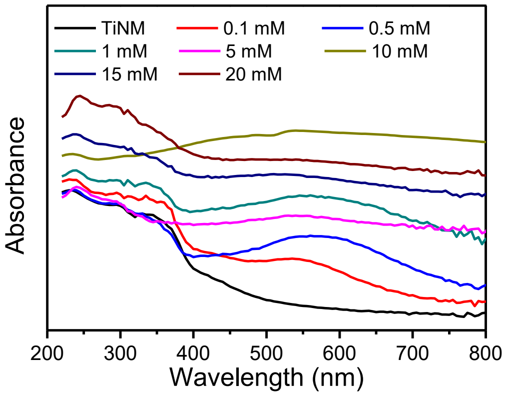

Fig. S6 UV/visible diffuse reflectance spectra of TiNM before and after decorating with AuNPs in different concentrations of $HAuCl_4$.

The influence of power densities for photothermal effect

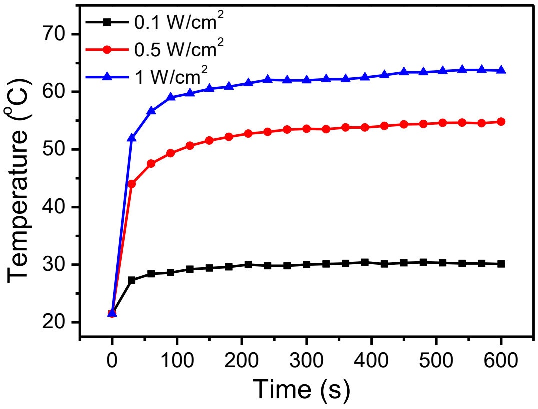

Fig. S7 Temperature rise of Au/TiNM irradiated with an NIR-light laser under different power densities.

It was found that the photothermal effect depends on the power density. When the irradiation power density was 1.0 W cm^{-2}, the final temperature of Au/TiNM increased to 60 °C in the first 100 s.

The influence of annealing time for photothermal effect

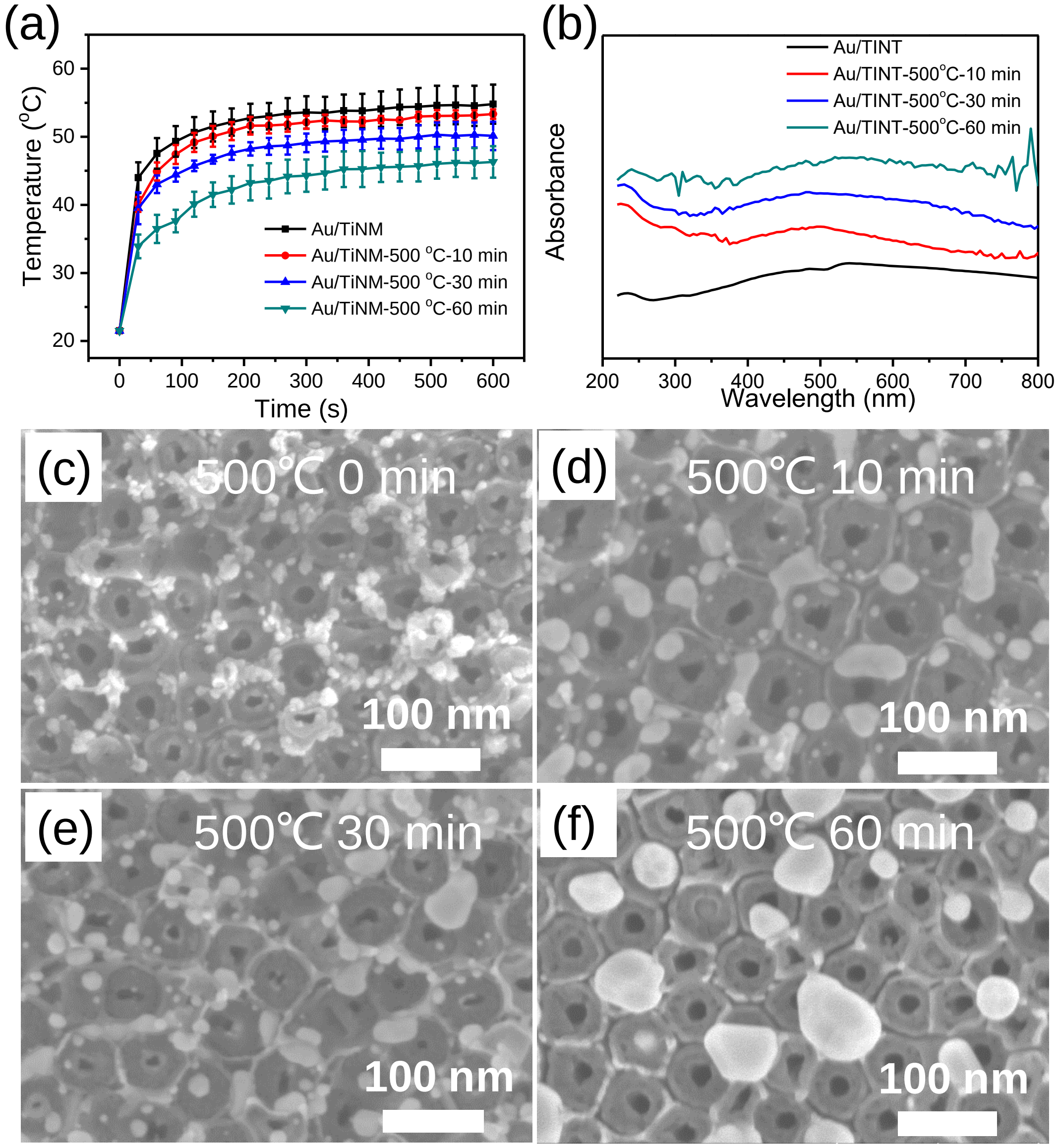

Fig. S8(a) Temperature rise of Au/TiNM before and after annealing at 500 °C for different periods. (b) The UV/visible diffuse reflectance spectra of Au/TiNM before and after annealing treatment at 500 °C for different periods. (c–f) SEM images of Au/TiNM before and after annealing treatment at 500 °C for different periods.

Figure S8 shows the effect of annealing time on the photothermal ability of Au/TiNM. We compared the photothermal conversion ability of Au/TiNM samples with annealing treatment for different times (10 min, 30 min, and 60 min). The temperature decreased with the increase in annealing time (Fig. S8a). The UV/visible diffuse reflectance spectra show that the intensity of absorption peak increased with the annealing time (Fig. S8b). The SEM images also show that the AuNPs became larger with the increase in annealing time (Figs. S8c–f). The change in diameter of AuNPs is consistent with the UV/visible diffuse reflectance spectra shown in Fig. S8b.[7]

The *I–V* curves for Au/TiNM

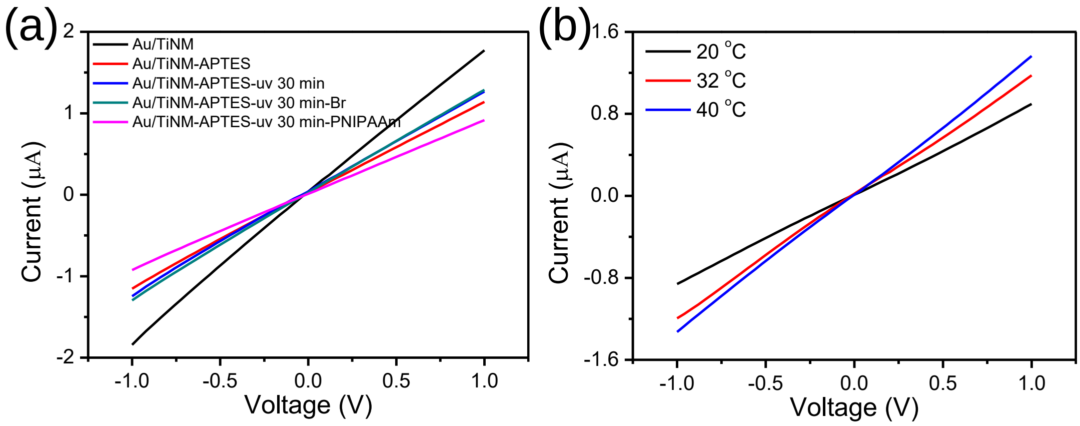

Fig. S9 *I–V* curves. (a) *I–V* curves corresponding to the modification of Au/TiNM-PNIPAAm nanochannels. (b) *I–V* curves for the Au/TiNM-PNIPAAm nanochannels at different temperatures.

The ionic transport properties of Au/TiNM nanochannels before and after chemical modification were evaluated by the corresponding Current–Voltage (*I–V*) curves in 1 mM KCl electrolyte solution. After modifying the terminal NH_2 groups on Au/TiNM, a decrease in the conductance of nanochannel system was observed (red line). After the nanochannels were placed in UV light for 30 min, an increase in the ionic current of nanochannel arrays was observed (blue line). This is related to the change in the surface charge of nanochannels, as confirmed by zeta potential data shown in Table S1. After the polymerization reaction, the ion conductance of nanochannels system decreased further (fuchsia line). These results show the successful modification of PNIPAAm onto the nanochannels. Fig. S9b shows the *I–V* curves of PNIPAAm brushes modified Au/TiNM at different temperatures. At RT (20 °C), the PNIPAAm brushes are swollen, thus decreasing the effective cross-section of nanochannels. This can be described by the low slope of *I–V* curves, indicating a low conductance of nanochannels (black line). An increase in the temperature above the lower critical solubility temperature can promote drastic changes on the conformational state of PNIPAAm brushes. In this case, the brushes suffer a transition into collapsed state, which caused a high conductance of the nanochannels (blue and red line).

The *I–V* curves for TiNM

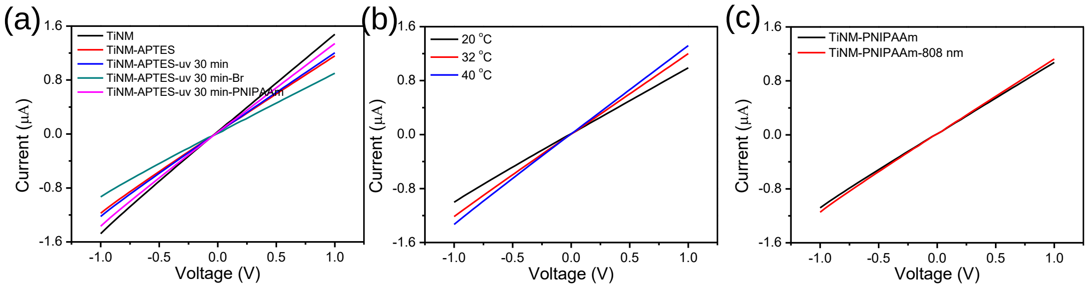

Fig. S10) *I–V* curves of TiNM in each preparation process for PNIPAAm modification. (b) *I–V* curves for PNIPAAm-decorated TiNM at different temperatures. (c) *I–V* curves for PNIPAAm-decorated TiNM before and after NIR-light laser irradiation for 300 s.

Figure S10a shows the control experiments using bare TiNM without AuNPs grafting. Ionic transport properties of the TiNM nanochannels system before and after chemical modification were examined from the corresponding *I–V* curves (Fig. S10a). The changes in current can be attributed to the changes in surface charge of nanochannels, as shown in Table S2. After attaching the PNIPAAm brushes onto the TiNM nanochannels surface, a low ionic conductance of nanochannels was observed (Fig. S10a, fuchsia line). The *I–V* curves of PNIPAAm-decorated TiNM at different temperatures show that the nanochannels fabricated here have temperature-responsive characteristics (Fig. S10b). However, when the nanochannels were irradiated with NIR-light for 300 s, the *I–V* curves do not show obvious changes. These results show that PNIPAAm brushes modified TiNM has no NIR response in the absence of AuNPs.

The *I–V* curves for Au-PNIPAAm-base/TiNM

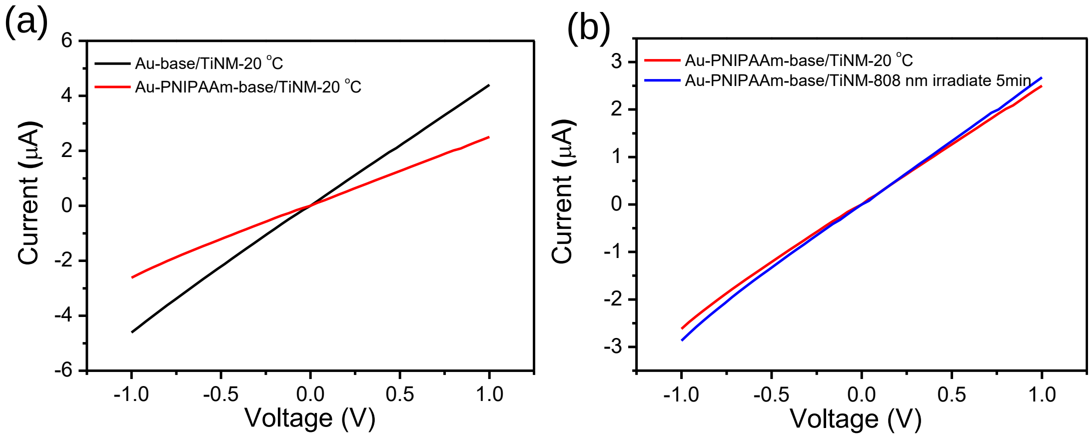

Fig. S11 (a) *I–V* curves for PNIPAAm-decorated on large base side of Au-base/TiNM. (b) *I–V* curves for PNIPAAm-decorated on large base side of Au-base/TiNM before and after NIR-light laser irradiation for 300 s.

To study the effect of nanochannels pore size on ion penetration, the AuNPs and PNIPAAm brushes were attached onto the large base side of TiNM (Au-PNIPAAm-base/TiNM) surface. Ionic transport properties of this system before and after PNIPAAm modification were evaluated based on the corresponding *I–V* curves. As shown in Fig. S11a, a low ionic conductance of nanochannels was observed after PNIPAAm modification, which is consistent with the result of modifying PNIPAAm at the small tip side of Au/TiNM recoded in Fig. S9a owing to the change of wettability and surface charge. However, after 808-nm laser irradiation for 300s, the *I-V* properties only exhibit a poor response (Fig. S11b) for the conformation change of PNIPAAm due to the large size of the base side.

The data of Zeta potential

Table S1. Zeta potential of the Au/TiNM in each preparation process for PNIPAAm modification in 1 mM KCl solution

Sample	Au/TiNM	Au/TiNM-APTES	Au/TiNM-APTES-UV-30 min	Au/TiNM-APTES-UV -30 min-Br	Au/TiNM-PNIPAAm
Zeta Potential (mV)	-28.40	-4.02	-13.10	-9.25	-3.96

Table S2. Zeta potential of the TiNM in each preparation process for PNIPAAm modification in 1 mM KCl solution

Sample	TiNM	TiNM-APTES	TiNM-APTES-UV-30 min	TiNM-APTES-UV-30 min-Br	TiNM-PNIPAAm
Zeta Potential (mV)	-8.26	5.26	-19.50	-10.20	-8.70

Reference

(1) Y. Y. Song, H. Hildebrand and P. Schmuki, *Surf. Sci*,. 2010, **604**, 346.

(2) S. Mohajernia, A. Mazare, E. Gongadze, V. Kralj-Iglic, A. Iglic and P. Schmuki, *Electrochim. Acta,* 2017, **245**, 25.

(3)T. Kiyonaga, T. Mitsui, M. Torikoshi, M. Takekawa, T. Soejima, H. Tada, *J. Phys. Chem. B,* 2006, **110**, 10771.

(4) J. W. Xu, X. M. Zhou, Z. D. Gao, Y. Y. Song and P. Schmuki, *Angew. Chem. Int. Ed,* 2015, **54**, 1.

(5) Y. Jiang, N. Liu, W. Guo, F. Xia and L. Jiang, *J. Am. Chem. Soc.,* 2012, **134**, 15395.

(6) Y. Y. Song, H. Hildebrand and P. Schmuki, *Electrochim. Acta,* 2009, **11**, 1429.

(7) J. E. Millstone, S. Park, K. L. Shuford, L. Qin, G. C. Schatz, C. A. Mirkin, *J. Am. Chem. Soc.*, 2005, **127**, 5312.